Engineered Science
DOI: https://dx.doi.org/10.30919/es1516

Quercetin Nanoarchitectures with Dual Bioactivity: Synergistic Antioxidant and Antibacterial Efficacy

Yewen Shen,[1] Jiawei Yao,[1] Dongjie Shi,[1] Jiyuan Li,[1] Jingshuai Liu,[1] Houjuan Qi,[1,*] Mohamed Kallel[2,*] and Zhanhua Huang[1,*]

Abstract

Quercetin (QT), a naturally flavonoid compound, demonstrates potent antioxidant capacity and diverse bioactivities. However, its pharmaceutical utilization is substantially constrained by intrinsic physicochemical limitations, including aqueous insolubility, low systemic bioavailability, and chemical lability. To address these challenges, this study developed multifunctional nanoparticles (QT-TA-ZA NSs) through ultrasonic self-assembly and zinc ion-mediated crosslinking strategies utilizing QT, tannic acid (TA), and zinc acetate (ZA). Characterization data revealed that the optimized QT-TA-ZA NSs exhibited the particle size of 200.9 ± 3.6 nm with high encapsulation efficiencies of 87.47 ± 0.35% for QT and 81.24 ± 0.43% for TA. The QT-TA-ZA NSs demonstrated pH-responsive release kinetics, achieving cumulative release rates of 68.73% (QT) and 73.91% (TA) at pH 4.8 over 24 h. Synergistic radical scavenging capabilities against DPPH·, $ABTS^{+}$, and hydroxyl radicals were observed, attributable to the antioxidant-rich phenolic hydroxyl networks within the QT-TA-ZA architecture. More significantly, QT-TA-ZA NSs exhibited outstanding antibacterial activities against Staphylococcus aureus and Escherichia coli. This work pioneers a nanoarchitectonics strategy to overcome QT's bioavailability barriers while integrating multifunctionality. The demonstrated pH-modulated drug release, ROS-scavenging capacity, and concentration-dependent bactericidal effects validate their translational potential in targeted antimicrobial therapies and oxidative stress mitigation.

Keywords: Self-assembly; Ion-crosslinking; Antioxidation.
Received: 24 March 2025; Revised: 25 April 2025; Accepted: 05 May 2025.
Article type: Research article.

1. Introduction

Quercetin (QT), a polyhydroxy flavonoid compound, is ubiquitously distributed across diverse botanical tissues including floral structures, fructus, and foliar systems.[1] However, its inherent hydrophobic characteristics and instability in the physiological environment lead to low bioavailability, which severely restricts its clinical translational applications. However, its clinical translation is substantially impeded by intrinsic physicochemical limitations, particularly pronounced hydrophobicity and chemical instability under physiological conditions, which collectively contribute to suboptimal pharmacokinetic profiles and markedly diminished bioavailability.

[1] *Key Laboratory of Bio-based Material Science & Technology, Material Science and Engineering College, Northeast Forestry University, Harbin, 150040, China*
[2] *Department of Physics, College of Science, Northern Border University, Arar, 73222, Saudi Arabia*
* *Email*: 15006383472@163.com (H. Qi);
Mohamed.Kallel@nbu.edu.sa (M. Kallel);
huangzh1975@163.com (Z. Huang)

Contemporary pharmaceutical nanotechnology has propelled the development of nanoengineered platforms for phytochemical encapsulation and targeted delivery, with the rational design of ecocompatible,[2] biosafe, and therapeutically optimized nanocarriers garnering significant research momentum in advanced drug delivery systems.[3,4] Despite advancements in conventional methodologies persistent challenges remain regarding their compromised biodegradation profiles and propensity for systemic accumulation-mediated inflammatory cascades.[5,6]

Recently, the self-assembly strategy has been extensively investigated and implemented in the realm of nanotechnology to tackle the aforementioned issues.[7] Self-assembly refers to the spontaneous formation of ordered structures by chaotic fundamental elements driven by non-covalent interactions. In this manner, bioactive materials could self-assemble into a supramolecular structure without any other carrier matrix, such as nanoparticles, gels and micelles.[8,9] Interestingly, such structure would break up when it is exposed to a particular environment, then releasing the bioactive materials and exerting their medicinal effect.[10] According to previous studies, Sun et al employed ultrasonic-triggered irreversible

equilibrium-tending self-assembly co driven with ionic cross-linking to fabricate multifunctional cinnamaldehyde-tannic acid-zinc acetate nanospheres. This synthetic strategy successfully achieved the integration of hydrophilic and hydrophobic small molecules.[11]

Here, QT and tannic acid (TA) were selected to co-assemble into nanoparticles. Also, to improve their stability and bioactivity, zinc acetate was used to crosslink the nanoparticles (QT-TA-ZA NSs) by forming a metal-polyphenol network structure.[12] The present study comprehensively evaluated the physical-chemical properties, microstructure, release behavior, stability, antibacterial activity, and antioxidant capacity of QT-TA-ZA NSs. The overarching objective was to engineer a multifunctional nanosystem featuring robust stability, superior dispersibility, and potent antibacterial and antioxidant capabilities. The results indicated that, in the absence of any chemically synthesized surfactants or carrier materials, the self-assembly attributes between QT and TA under ultrasonic treatment not only facilitated their assembly, thereby enhancing functionality, but also notably improved the stability and bioavailability of plant-derived polyphenol bioactive molecules. These findings offer exceptional nano-modifiers and modification materials for the rational design of green, multifunctional, and degradable materials, thus contributing to the advancement of sustainable materials science.[13]

2. Experimental sections

2.1 Preparation of QT-TA-ZA NSs

Initially, ethanolic solutions of QT at varying concentrations were prepared and introduced via dropwise addition into 5 mL of 1 mg/mL tannic acid (TA) aqueous solution under 800 W ultrasonic irradiation, yielding crude QT-TA nanoemulsions (QT-TA NEs). The colloidal characteristics of QT-TA NEs were systematically evaluated using dynamic light scattering to determine the optimal QT loading capacity. Subsequently, 1 mL aliquots of zinc acetate (ZA) solutions at graded concentrations were incorporated into the optimized QT-TA NEs, followed by ultrasonic crusher (800 W, 20 min) to facilitate the formation of QT-TA-ZA nanospheres (QT-TA-ZA NSs). The optimal ZA concentration was selected according to changes in particle size, Zeta potential, and UV-absorption spectra. The suspension was centrifuged at 10000 rpm for 10 min, and the QT-TA-ZA NSs were washed three times with ultrapure water to remove uncrosslinked monomers. Finally, the QT-TA-ZA NSs powder was obtained via freeze-drying.

2.2 Dynamic light scattering test

The particle size of the nano-emulsion was determined by DLS, and the ζ- potential of the nano-emulsion was determined by inserting an electrode. The samples were prepared twice under the same conditions, and each sample was repeated for 3 times. The average ζ- potential, particle size and PDI were calculated.

2.3 Microscopic morphology

The QT-TA-ZA NSs was diluted with ultra-pure water, and then dripped onto a silicon wafer and dried at 60 °C for 2 h to remove the moisture. The sample is then sprayed with platinum for 3 min using a sputtering deposition device. The microscopic morphology of QT-TA-ZA NSs was observed by scanning electron microscope (Thermo Scientific, USA) and transmission electron microscope (Thermo Scientific, USA).

2.4 UV-vis spectroscopy and FT-IR

Fourier transform infrared (FT-IR) spectroscopy is a reliable technique used to determine the structure of chemical bonds. The change in the electron cloud distribution of the benzene ring conjugate system caused by intermolecular interactions usually leads to changes in the ultraviolet-visible absorption spectrum.[14] The interactions among various components of QT-TA-ZA NSs were investigated using an ultraviolet spectrophotometer (TU-1950, Beijing, China) and a FT-IR spectrometer. For the UV spectrum, the wavelength range is 200 ~ 800 nm. The types of functional groups on the surface of samples were qualitatively analyzed by FT-IR. Scanning range is 4000 ~ 515 cm^{-1}, resolution is 4 cm^{-1}, and scanning frequency is 32 times.

2.5 XRD analysis of QT-TA-ZA NSs

X-ray diffraction is widely used to evaluate the crystallinity of nanomaterials and the presence of interactions between different components during synthesis.[15] The crystal structure of QT-TA-ZA NSs was evaluated by the X-ray diffractometer (XRD, XRD 6100, Shimadzu Company, Japan). The scanning angle range and scanning speed were set to 5 ~ 80° and 5° min^{-1}, respectively.

2.6 Encapsulation efficiency determination of QT and TA

Encapsulation efficiency (EE) is generally considered to be an important indicator for evaluating the effectiveness of nanodrug delivery systems.[16] In this study, UV-vis spectrophotometry was used to quantitatively analyze the encapsulation efficiency of QT and TA in QT-TA-ZA NSs. The specific operation is as follows: Take the freshly prepared nanosuspension and centrifuge it at a high speed (10000 rpm, 10 min). After separation, collect the supernatant for the determination of the concentration of unencapsulated drugs. The standard curves of QT and TA were calculated by Eqs. (1) and (2):

$$\text{QT},\ y = 0.00048x + 0.00525,\ R^2 = 0.998 \quad (1)$$

$$\text{TA},\ y = 0.00039x + 0.006286, R^2 = 0.999 \quad (2)$$

where y was the absorbance at the absorption peak of the liquid phase of the supernatant, and x was the concentration of QT or TA. The EE was calculated by Eq. (3):

$$EE(\%) = \frac{(W_0 - W_1)}{W_0} \times 100\% \quad (3)$$

where W_0 was the initial mass (mg) of the added bioactive

ingredient (QT or TA) and W_1 was the mass (mg) of the unencapsulated QT or TA in the system.

2.7 Controlled release performance of QT-TA-ZA NSs

The natural physiological pH of the epidermis in healthy individuals is maintained within a slightly acidic range. The pH on the skin surface is usually between 4.5 and 5.3.[17,18] After skin damage, its pH value may rise to neutral. We selected phosphate buffer solutions with pH values of 4.8 and 6.8 as simulated solutions for sustained drug release for QT-TA-ZA NSs. Briefly, 8 mg of QT-TA-ZA NSs were loaded into a dialysis bag. Subsequently, the dialysis bag was immersed in 30 mL of PBS solutions with pH values of 4.8 and 6.8, respectively. The system was then oscillated at 37 °C with a rotation speed of 150 rpm/min. At specific time intervals, 3 mL of the sustained-release solution was taken out, and its absorbance was measured. To maintain the constant volume of the release system, 3 mL of fresh buffer solution was added to the sustained-release system. The *in vitro* drug release curve was plotted based on the cumulative release rate. The cumulative release (CR) of TA or QT was calculated using the following Eq. (4):

$$Cumulative\ ralease(\%) = \frac{V_0 \sum_1^{n-1} C_i + C_n V_1}{m_0} \times 100\% \quad (4)$$

where V_0 represents the volume of each sample, V_1 denotes the total volume of the added buffer solution, mL. C_i is the concentration of QT-TA-ZA NSs at the time of sampling, and C_n represents the concentration of QT-TA-ZA NSs in the release solution extracted at the corresponding time, mg/mL. m_0 is the content of QT-TA-ZA NSs, mg.

2.8 Storage stability

The stability of 10 μg/mL QT-TA-ZA NSs was evaluated at 4 °C. To observe the release properties of QT and TA in aqueous solution, the ultraviolet spectra of QT-TA-ZA NSs were collected at different intervals (0, 1, 3, 5, 7, and 10 days).

2.9 Antioxidation properties

The antioxidation properties were evaluated using the DPPH• method,[19] $ABTS^+$ method,[20] and hydroxyl radicals (•OH) scavenging activity. The DPPH• solution (2×10^{-4} M) was prepared. 2 mL DPPH• solution and different QT-TA-ZA NSs concentrations were added to the test tube, and stored at room temperature in the dark. After 30 min, the absorbance of the solution at 517 nm was measured using an Uv-vis spectrophotometer. The free radical scavenging activities of QT-TA-ZA NSs was calculated as following Eq. (5):

$$DPPH\bullet\ \text{scavening activity}\ (\%) = \frac{(A_0 - A_i)}{A_0} \times 100\% \quad (5)$$

where A_0 was the absorbance of control, and A_i was the absorbance of the different QT-TA-ZA NSs ($n \geq 5$).

Meanwhile, the $ABTS^+$ radical scavenging activity was tested following the kit's instructions. The different QT-TA-ZA NSs concentrations were added into a 96-well plate. 200 μL $ABTS^+$ solution was placed into each well. The absorbance (λ = 734 nm) of the sample solution was measured using a microplate reader (FlexA-200, Hangzhou Aosheng, China). The free radical scavenging activities of QT-TA-ZA NSs was calculated as following Eq. (6):

$$ABTS^+\ \text{scavening activity}(\%) = \frac{B_0 - B_i}{B_0} \times 100\% \quad (6)$$

where B_0 and B_i were the absorbance values of the control and experimental group, respectively.

The determination of the scavenging activity of free radicals (•OH) was carried out using the optimized method of the Fenton reaction system reported in reference.[21] Firstly, the different QT-TA-ZA NSs concentration gradients were accurately transferred into 10 mL test tubes. 1 mL 9 mmol/L ferrous sulfate solution and 1 mL 9 mmol/L ethanol-salicylic acid solution were successively added to each tube. After thorough mixing, 1 mL 8 mmol/L hydrogen peroxide solution was introduced. The test tubes were then placed in a thermostatically controlled water-bath shaker set at 37 °C. The samples were incubated in the dark at a shaking speed of 120 rpm for 30 minutes to ensure a complete reaction. Following the incubation period, the absorbance of each sample was measured at a wavelength of 510 nm using an Uv-vis spectrophotometer. Specifically, the absorbance of the experimental samples was denoted as A_1. For the positive control group, where the QT-TA-ZA NSs were replaced with an equal volume of a vitamin C solution, the absorbance was recorded as A_2. In the control group, where the hydrogen peroxide solution was substituted with an equal volume of deionized water, the absorbance was marked as A_3. Formulated to measure the clearance rate with the above conditions, the calculation formula is as following Eq. (7):

$$\bullet OH\ elimination\ (\%) = \left(A_2 - \frac{A_1 - A_3}{A_2}\right) \times 100\% \quad (7)$$

where A_1 is the absorbance of the added sample, A_2 is the control group, and A_3 is the blank control group.

2.10 Antibacterial activity

The emergence of multidrug-resistant microorganisms and the associated outbreaks pose significant threats to humanity, compelling the active exploration of alternative strategies aimed at developing novel antimicrobial agents that can be effectively deployed across multiple cycles.[22] In this experiment, Gram-positive Staphylococcus aureus (*S. aureus*) and Gram-negative Escherichia coli (*E. coli*) were mainly used as models to study the *in vitro* antibacterial activity of QT-TA-ZA NSs.[23] The specific procedures are as follows:

(1) Minimum Inhibitory Concentration (MIC): In order to explore the sensitivity of bacteria to the drug, the bacteria were diluted 10^5 to 10^6 times with normal saline. The diluted bacteria (150 μL) were transferred into the prepared medium (nutrient agar: PBS = 1:1), and QT-TA-ZA NSs at different concentrations were added. The mixture was incubated in a constant-temperature shaking flask in a gas bath at 37 °C for

18 h. Then, the clarity of the solution was observed, and the concentration corresponding to the solution that became clear first was determined as the minimum inhibitory concentration. In addition, the antibacterial effect of QT-TA-ZA NSs against *S. aureus* and *E. coli* was evaluated by the plate counting method. The antibacterial experiment was carried out at the minimum inhibitory concentration measured in the previous experiment.

(2) Antibacterial Zone Experiment: The bacteria were diluted 10^5 to 10^6 times with normal saline. Then, 150 μL of the diluted bacterial suspension was taken and evenly inoculated onto the surface of an agar plate using a sterile spreading rod. The prepared QT-TA-ZA NSs samples were soaked on filter paper discs with a diameter (d) of 1 cm. After the filter paper discs were saturated with the samples, they were placed in the middle area, and then cultured in a sterile box at 37 °C for 24 h. Finally, the size of the antibacterial zone was observed.

3. Results and discussion

3.1 Synthesis of QT-TA-ZA NSs

Self-assembly of bioactive molecular opens a new window for the development of nanomaterials and improvement of their bioactivity.[24] The QT-TA-ZA NSs were successfully prepared in a uniformly dispersed state by leveraging the self-assembly property between QT and TA. Subsequently, they were further cross-linked by metal ions to form a metal-polyphenol network. (Fig. 1a) When QT was added to the TA solution, the color of the QT-TA NEs transformed from colorless to milky yellow (Fig. 1b). This phenomenon indicates that, without the presence of any surfactants, QT and TA can self-assemble into nanoparticles with the assistance of ultrasonic waves. Fig. 1c and Fig. S1a showed the average droplet size, Zeta potential, and PDI values of QT TA NEs with different QT contents. When the QT concentration was 2 mg/mL, the smallest particle size of 398.3 ± 5.78 nm was obtained, and its PDI value was 0.27 ± 0.003, indicating that the suspension was in the most stable state at this concentration.

A characteristic absorption peak at approximately 265 nm appears between the characteristic absorption peak of TA at 275 nm and that of QT at 254 nm (Fig. 1e), which proved the existence of an interaction between QT and TA. The introduction of ZA could trigger a strong ionic cross-linking reaction among TA, QT, and metal ions (Zn^{2+}), thus forming QT-TA-ZA NS. With the increased of ZA content, the characteristic absorption peak intensity at 265 nm of the QT-TA-ZA NSs were decreased. As the ZA concentration increased, its absorbance intensity gradually decreased. When the ZA concentration reached 0.12 mol/L, the absorbance intensity reached its minimum value. The results of size distribution demonstrated that the concentration of ZA increased from 0.02 M to 0.06 M, the particle size of the QT-TA-ZA NSs decreased from 937.5 nm to 328.5 nm, the PDI value and zeta potential also gradually decreased (Fig. 1d and Fig. S1b). When the concentration of ZA was 0.12 M, the particle size of QT-TA-ZA NS was the smallest (200.9 nm) and the PDI value was 0.23. However, when the concentration of ZA further increased to 0.3 M, the particle size reached microns. This was because as the number of metal ions in the system increases, excessive free metal ions did not participate in cross-linking. The surface viscosity of the particles increased, and the diffusion of lipophilic components in the aqueous phase was inhibited, leading to agglomeration and flocculation.[25,26] Therefore, 2 mg/mL QT and 0.12 M ZA were selected for further study.

To further understand the microscopic morphology of the QT-TA-ZA NSs, TEM and SEM were employed (Fig. 1f). QT-TA-ZA NSs presented as uniform irregular spherical nanoparticles. The formation mechanism of the QT-TA-ZA NSs was explored. It is likely that the ionic cross-linking between ZA, QT, and TA caused the original small particles to aggregate into larger units. In addition, the stability of QT-TA-ZA NSs was also evaluated. The characteristic Uv-vis absorption spectrum intensity gradually increased with the increase of the storage time and reached equilibrium on the 10th day, revealing the sustained-release pattern of the bioactive components (QT and TA) in QT-TA-ZA NSs (Fig. 1g). Moreover, the morphology of the QT-TA-ZA NSs showed no change after 10 days of storage (Fig. S2), further confirming the excellent stability of the nanoparticles, which is beneficial for improving their bioavailability.

3.2 Characterization of QT-TA-ZA NSs

FT-IR, XRD and XPS were used to investigate the chemical structure of QT-TA-ZA NSs. The vibration modes exhibited by various functional groups of the prepared QT-TA-ZA NSs were analyzed in Fig. 2a. FT-IR spectra demonstrated that the characteristic peaks of both QT and TA were retained in QT-TA-ZA NSs. These included the aromatic ring C=C stretching vibration peaks at 1611 cm^{-1}, 1562 cm^{-1}, and 1461 cm^{-1}, as well as the C-H vibration peaks at 1319 cm^{-1}, 1269 cm^{-1}, and 1200 cm^{-1}.[27,28] Compared to TA and QT, the hydroxyl group vibration peak of QT-TA-ZA NSs in the range 3200 ~ 3550 cm-1 decreased significantly, indicating a strong interaction between Zn^{2+} and hydroxyl group.[29,30] These results confirm the successful coordination of Zn^{2+} with QT and TA within the QT-TA-ZA nanosheets NSs, driving the formation of a cross-linked architecture.

To explore the crystal structure of the QT-TA-ZA NSs, the XRD technique was used. Fig. 2b displayed the XRD patterns of QT-TA-ZA NSs and TA. TA exhibited typical amorphous characteristics, with a broad characteristic diffraction peak appearing at 14.2°. Due to the excellent crystallinity of ZA, a sharp and prominent crystallization diffraction peak emerged at 12.5°, corresponding to the (200) characteristic crystal plane of ZA. QT also has good crystallinity, with the maximum diffraction intensity appearing at 27.3°. The XRD pattern of QT-TA-ZA NSs showed diffraction peak at 2θ = 12.5° and 27.3°, indicating that Zn^{2+} and QT were successfully introduced into the nanoparticles.[31,32] The XRD results were

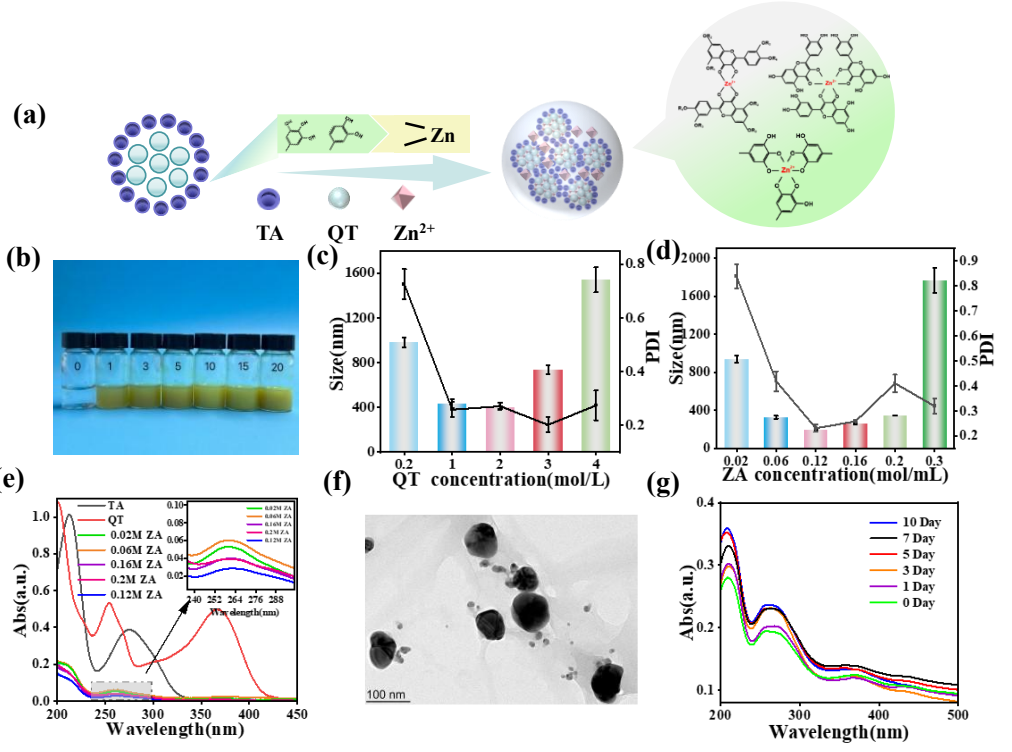

Fig. 1: (a) The possible formation mechanism of QT-TA-ZA NSs, (b) The photograph of the TA-ZA NEs, (c) Particle size distribution of QT-TA-ZA NSs with different QT concentrations, (d) Particle size distribution of QT-TA-ZA NSs at different ZA concentrations, (e) UV-vis spectrum of TA-ZA NSs with different amounts of ZA concentrations. (f) TEM diagram of QT-TA-ZA NSs. (g) UV absorption spectra of TA-ZA NSs at different days.

consistent with those of FT-IR, which further indicated that QT-TA-ZA NSs was successfully synthesized.

To clarify the elemental composition, valence state, and chemical bonds, the X-ray photoelectron spectroscopy (XPS) spectra of the QT-TA-ZA NSs are shown in Fig. 2.[33] The C, O and Zn elements were detected on the surface of the QT-TA-ZA NSs (Fig. 2c). In the high-resolution O1s spectrum (Fig. 2d), the three peaks at 531.6 eV, 285.1 eV, and 288.3 eV are assigned to Zn-O, C-O, and C=O, respectively. The peak at 532.3 eV is assigned to O-H, which proves that the QT-TA-ZA NSs have a hydroxyl-rich structure. In the high resolution C1s spectrum (Fig. 2e), the electron binding energies of carbon are 284.2 eV, 286.1 eV, and 288.3 eV, corresponding to C-C, C-O, and O-C=O, respectively. Additionally, in the high-resolution Zn2p spectrum (Fig. 2f), two binding energies of 1045.6 eV and 1021.2 eV were identified, corresponding to $Zn2p_{2/1}$ and $Zn2p_{3/2}$, respectively.[33,34] In XPS analysis, the carbon-to-oxygen ratio is often used to characterize the oxidation state of the material surface or the composition of functional groups. The chemical formula of TA is $C_{76}H_{52}O_{46}$, and the chemical formula of QT is $C_{15}H_{10}O_7$. In the prepared QT-TA-ZA NSs, the C/O ratio is 70.14:28.16, and the carbon-to-oxygen ratio of the QT-TA-ZA nanoparticles is higher than that of the two raw materials. In polyphenolic nanomaterials, the hydroxyl groups (-OH) and quinone groups (-C=O) of TA contribute to a relatively high oxygen content, and the polyhydroxyl structure of QT is also rich in oxygen elements. The fact that the C/O ratio of the nanoparticles is higher than that of the QT and TA monomers indicate that, under the dominance of hydrophobic interactions: TA and QT combine through π-π stacking or hydrophobic interactions, reducing the exposure of oxygen-containing functional groups.[35] At the same time, the coordination of metal ions Zn^{2+} with the polyphenolic hydroxyl groups of TA may change the chemical environment of oxygen (forming Zn-O bonds), indirectly affecting the C/O ratio.[36] These results were further confirmed the successful introduced Zn ions into the nanoparticles and strong interaction formed between Zn and phenolic hydroxyl groups in TA and QT.[37] The results of XPS were consistented with those of XRD and FT-IR, further demonstrating the successful synthesis of QT-TA-ZA NSs.

3.3 *In vitro* drug release behavior and mechanism study

EE of QT and TA was determined via measuring the UV absorbance of supernatant at 265 nm and 374 nm, respectively. The EE of QT and TA in QT-TA-ZA NSs were 87.47 ± 0.35% and 81.24 ± 0.43%, respectively (Figs. 3a-b). These results indicated the effectiveness and feasibility of the prepared drug delivery system. The drug release rate at different pH was operated to determine the controlled-release performance of QT-TA-ZA NSs (Figs. 3c-d). It can be observed that the drug release exhibits a two-stage kinetic characteristic: a rapid release occurs in the initial stage, followed by a slow and sustained release process. Within the first 20 hours, QT-TA ZA NSs exhibit a relatively fast release rate. When the condition changed from acidic condition to neutral condition, the

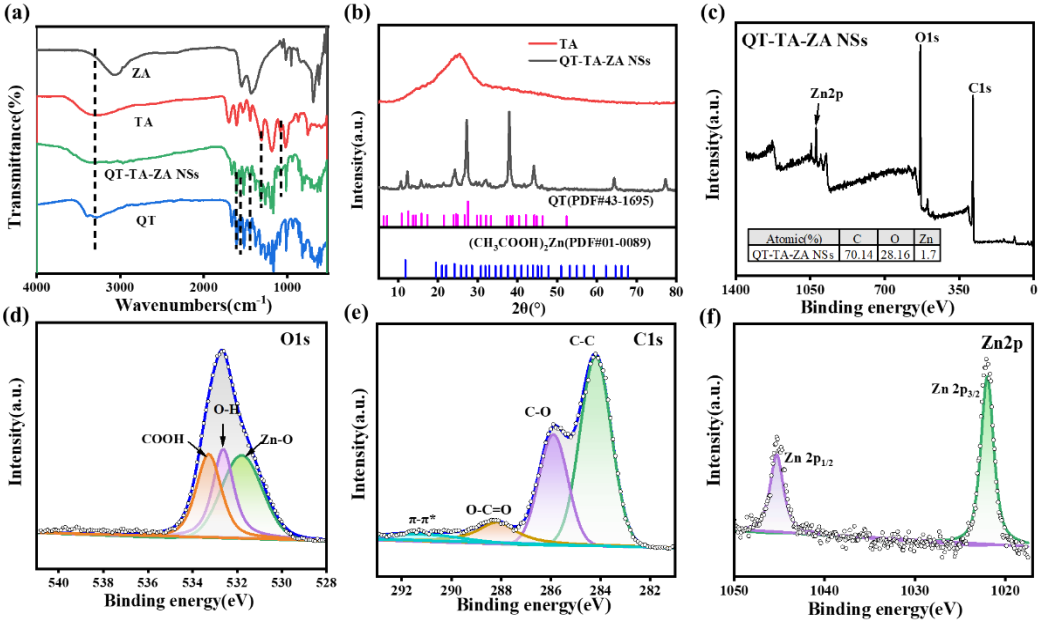

Fig. 2: Physicochemical structure of QT-TA-ZA NSs. (a) FT-IR spectra, (b) XRD patterns of QT-TA-ZA NSs, and the XPS survey spectrum (c), the high-resolution O1s spectrum (d), the high-resolution C1s spectrum (e), the high-resolution Zn2p spectrum (f) of the QT-TA-ZA NSs.

accumulation both QT and TA release were increased, that was from 68.73% to 73.91% for QT, from 64.17% to 82.57% for TA. Drug release from QT and TA showed good pH dependence. This could be attributed to Zn^{2+} tended to form coordination with both QT and TA under acidic condition, hence hinder its release.[38] These results proved that QT-TA-ZA NSs had a potential in controlled release, implied that its ability in clinical application. For instance, in response to pH alterations in damaged skin, the nanoparticles can be induced to release the active ingredients.[39]

To investigate the release mechanism of QT-TA-ZA NSs, the zero-order model, first-order model, Higuchi model, and Ritger-Peppas model were used to fit the time-dependent data of drug release. Analysis of the fitting results showed that the QT and TA release in the QT-TA-ZA NSs was controlled by drug diffusion (Figs. 4e-f, Figs. S3 and S4). The first-order kinetic model had the highest degree of fitting ($R^2 \approx 1$). This indicates that the release of active ingredients in QT-TA-ZA NSs drugs follows a first-order kinetic equation, which is consistent with Fick's diffusion. The driving force for diffusion is generated by the concentration gradient.

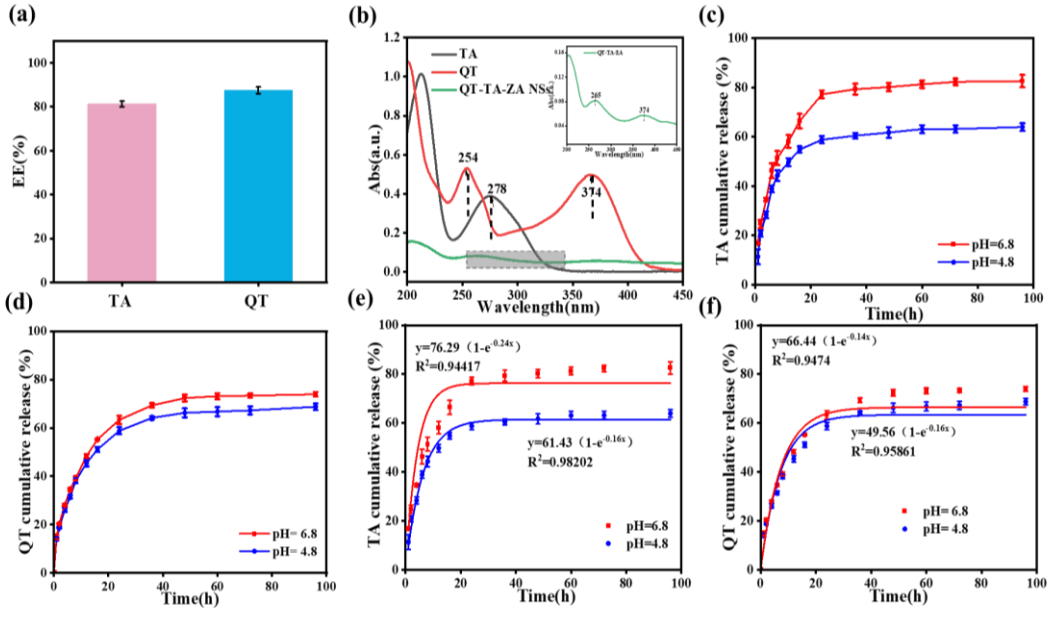

Fig. 3: (a) EE of QT-TA-ZA NSs. (b) UV spectrum curves of TA, QT, and QT-TA-ZA NSs. The cumulation release of (c) TA and (d) QT at pH = 4.8 and pH = 6.8. First-order drug release kinetics fitting curve of TA (e) and QT (f).

3.4 Antioxidant property of QT-TA-ZA NSs

QT and TA can achieve antioxidant effects by scavenging reactive oxygen species (ROS), chelating metal ions, and suppressing the oxidative damage of low-density lipoproteins.[40] Both QT and AT were rich in phenolic hydroxyl group. The DPPH molecule contains unpaired electrons, when it reacts with QT and TA, these unpaired electrons will be converted into a stable structure (N-H). The interaction between DPPH• and antioxidants involves the acceptance of hydrogen radicals, thus forming a DPPH-H complex. This transformation is accompanied by a color change from deep purple to light yellow. (Figs. 4a-b).[41] As the concentration of QT-TA-ZA NSs increased, the inhibitory effect on DPPH• also increased. When the concentrations of QT-TA-ZA NSs were 10, 20, 30, 40, 50, and 60 μg/mL, the scavenging efficiencies of DPPH• were 43.4%, 65.5%, 83.7%, 89.5%, 89.9%, and 89.8% respectively. A relatively high scavenging rate of DPPH• could be achieved with a low concentration of QT-TA-ZA NSs, which was the result of the synergistic effect of QT and TA. This result was attributed to the abundant polyphenol structures in QT and TA, which were conducive to rapidly capturing a large number of free radicals. Additionally, the $ABTS^+$ radical scavenging assay is another method for evaluating the antioxidant level. As the concentration of QT-TA-ZA NSs increased, the free radical scavenging activity gradually increased until it reached a stable state (Fig. 4c). The results show that when the concentration of QT-TA-ZA NSs was 40 μg/mL, the scavenging rate of $ABTS^+$ reached 91.36%.

The hydroxyl radical (•OH) is an important component of reactive oxygen species and possesses a strong electron-withdrawing ability. An excessive production of •OH can exceed the scavenging capacity of the intracellular antioxidant defense system, and subsequently attack biological molecules such as cell membrane phospholipids, proteins, and DNA.[42] As shown in Fig. 4d, QT-TA-ZA NSs exhibit excellent scavenging ability for •OH, and this scavenging ability gradually increased with the rise in concentration. When the concentration of QT-TA-ZA NSs is 600 μg/mL, the scavenging rate of •OH reached 74.4%. The result indicated that QT-TA ZA NSs possess outstanding free radical scavenging performance. This is because QT-TA-ZA NSs contain a high concentration of phenolic hydroxyl groups. The relatively low dissociation enthalpy of the O-H bond ensures that hydrogen atoms can be easily separated and act as hydrogen donors. These groups are able to react with the excessive free radicals generated in the body, thereby effectively alleviating oxidative stress.[43]

3.5 Antibacterial study of QT-TA-ZA NSs

The antibacterial properties of QT-TA-ZA NSs were evaluated by observing the inhibition zone and using the plate spreading method. Different gradient concentrations of QT, TA, and QT-TA-ZA NSs were used to detect their minimum inhibitory concentrations against Staphylococcus aureus (*S. aureus*) and Escherichia coli (*E. coli*) (Fig. S5). When the concentration of QT-TA-ZA NSs increased to 60 μg/mL, the test tube containing *S. aureus* became clear. When the concentration reached 80 μg/mL, the test tube containing *E. coli* became clear.

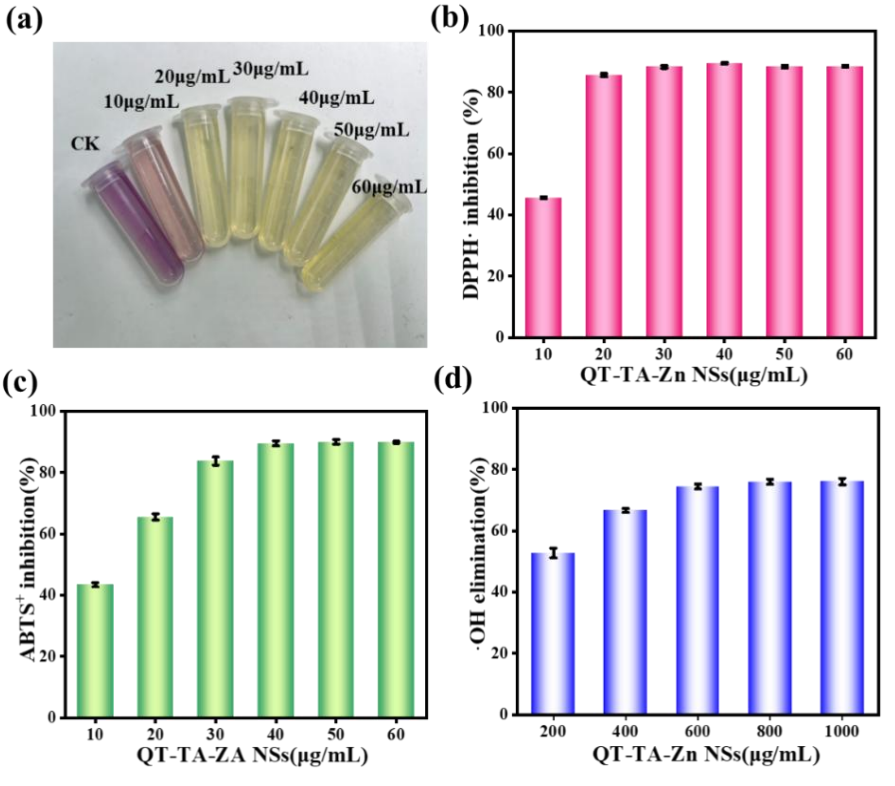

Fig. 4: Scavenging effect of QT-TA-ZA NSs evaluated by (a-b) DPPH•, (c) ABTS+, and (d) •OH scavenging assays.

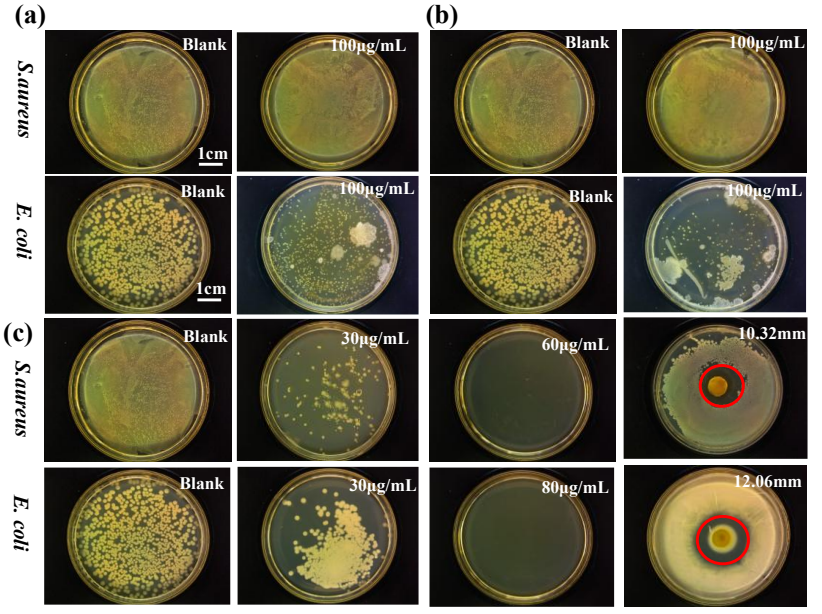

Fig. 5: Antibacterial capacities of QT-TA-ZA NSs. Photographs of bacteriostatic effect of (a) QT, (b) TA, and (c) QT-TA-ZA NSs.

The dilution-plating method was carried out to further observe the antibacterial effect (Fig. 5). It was clearly observed that the QT and TA samples had weak antibacterial abilities (Fig. 5a-b). On the contrary, low concentrations of QT-TA-ZA NSs exhibited strong antibacterial activity against both *S. aureus* and *E. coli* (Fig. 5c). To delve deeper into its antibacterial effect, antibacterial experiments were carried out by employing various concentrations of QT-TA-ZA NSs. As a result, the concentration-dependent antibacterial properties of QT-TA ZA NSs were clearly discernible. The antibacterial rates of 30 μg/mL QT-TA-ZA NSs against *E. coli* and *S. aureus* were 49.8% and 38.4%, respectively. When the concentration was increased to 60 μg/mL, the inhibition rate against *S. aureus* reached 100%. Subsequently, when the concentration reached 80 μg/mL, the inhibition rate against *E. coli* also achieved 100%.

Filter paper containing QT-TA-ZA NSs was placed in the middle of a petri dish for the inhibition zone experiment. After 24 h of incubation, the *S. aureus* and *E. coli* inhibition zones were 10.32 mm and 12.06 mm, respectively. This is mainly due to the antibacterial properties of TA and QT, Simultaneously, Zn^{2+} can further augment these antibacterial effects. Moreover, the metal-polyphenol network formed by TA, QT, and Zn^{2+} demonstrates remarkable broad-spectrum antibacterial characteristics.[44,45] TA, QT, and Zn^{2+} can penetrate the bacterial cell wall, causing changes in the cellular electrochemical potential and destroying the integrity of the cell membrane, Zn^{2+} can also disrupt the enzymes in the intracellular electron transport system and react with -SH groups, thus achieving the purpose of sterilization.[46]

4. Conclusion

In this study, the bioactive ingredients QT and TA were taken as the research objects. Exploiting the self assembly and ionic cross-linking properties, QT-TA-ZA NSs featuring remarkable antioxidant and antibacterial capabilities were expeditiously synthesized. The raw materials employed in the synthesis were characterized by their safety and biodegradability. The synthetic procedure was straightforward and environmentally friendly, adhering to ecological sustainability principles. The QT-TA-ZA NSs presented a well-dispersed spherical morphology and this structural feature facilitated the sustained release of functional components across a range of pH conditions. *In vitro* antimicrobial tests demonstrated that the successful loading of QT and TA endowed QT-TA-ZA NSs with broad-spectrum antimicrobial activity against *S. aureus* and *E. coli*. Upon reaching a concentration of 60 μg/mL for QT-TA-ZA NSs, the *S. aureus* antibacterial rate against to 100%. Subsequently, as the concentration further escalated to 80 μg/mL, the *E. coli* antibacterial rate against to 100%. Meanwhile, it had excellent scavenging performance on DPPH•, $ABTS^{+}$, and •OH, revealing its great potential in anti-bacterial infection, anti-oxidation and reducing oxidative stress damage. This study provides a new strategy for the construction of QT and TA multifunctional nano-systems and a new method for the construction of self-assembly nano-systems of plant-derived active ingredients. Its simple preparation, material safety and enhanced biological activity emphasize its clinical application potential.

Acknowledgments

This work was Supported by the Fundamental Research Funds for the Central Universities (Grant No. 2572022BB10), China Postdoctoral Science Foundation (Grant No. 2022TQ0059), Natural Science Foundation of Heilongjiang Province of China (Grant No. LH2024C045, and ZL2024C025). The authors extend their appreciation to the Deanship of Scientific Research at Northern Border University, Arar, KSA, for

funding this research work through the project number NBU-FFR-2025-2193-12.

Conflict of Interest

There is no conflict of interest.

Supporting Information

Applicable.

References

[1] O. D. Frent, D. M. Duda-Seiman, L. G. Vicas, N. Duteanu, N. S. Nemes, B. Pascu, A. Teusdea, C. M. Morgovan, M. E. Muresan, T. Jurca, A. Pallag, O. Micle, E. Marian, Study of the influence of the excipients used for the synthesis of microspheres loaded with quercetin: their characterization and antimicrobial activity, *Coatings*, 2023, **13**, 1376, doi: 10.3390/coatings13081376.

[2] L. V. Srinivasan, S. S. Rana, A critical review of various synthesis methods of nanoparticles and their applications in biomedical, regenerative medicine, food packaging, and environment, *Discover Applied Sciences*, 2024, **6**, 371, doi: 10.1007/s42452-024-06040-8.

[3] J. Sarris, Herbal medicines in the treatment of psychiatric disorders: 10-year updated review, *Phytotherapy Research*, 2018, **32**, 1147-1162, doi: 10.1002/ptr.6055.

[4] I. N. Zulayqha Nor Azmi, P. W. Chia, R. K. Liew, H. M. Yusoff, T. S. Chuah, F. S. Julius Yong, C. G. Joseph, Z. Guo, E. Buchar, Z. Wang, W. Winchester, E. Witherspoon, Biowastes as sustainable source for nanoparticle synthesis and their pesticide properties: a review, *ES Food & Agroforestry*, 2024, **16**, 1122, doi: 10.30919/esfaf1122.

[5] S. Qin, A. Zhang, S. Cheng, L. Rong, X. Zhang, Drug self-delivery systems for cancer therapy, *Biomaterials*, 2017, **112**, 234-247, doi: 10.1016/j.biomaterials.2016.10.016.

[6] A. Seilkhan, An overview of green applications of natural products for pharmaceutical, biofuel, and rubber industries: case study of Kazakh dandelion (taraxacum kok-saghyz Rodin.), *ES Energy & Environment*, 2024, **25**, 1171, doi: 10.30919/esee1171.

[7] L. Qiao, L. Yuan, S. Gao, Z. Wang, Y. Tang, C. Chen, C. Zhao, X. Fu, Self-assembled nanodrug delivery systems for anti-cancer drugs from traditional Chinese medicine, *Biomaterials Science*, 2024, **12**, 1662-1692, doi: 10.1039/D3BM01451G.

[8] R. D. Prasad, R. S. Prasad, R. B. Prasad, S. R. Prasad, S. B. Singha, R. J. Prasad, P. Sinha, B. U. M. B. India, S. Saxena, D. C. K. U. India, A. K. Vaidya, S. B. B Teli, U. R. Saxena, A. Harale, M. B. Deshmukh, M. N. Padvi, G. J. Navathe, A review on modern characterization techniques for analysis of nanomaterials and biomaterials, *ES Energy & Environment*, 2024, **23**, 1087, doi: 10.30919/esee1087.

[9] S. S. Gajbhiye, M. V. Salve, M. D. Gaikwad, A. R. Rasage, M. S. Khater, V. H. Ghadage, N. B. Chaure, Influence of synthesis conditions on the physical characteristics and antibacterial activities of cerium oxide nanoparticles in biomedical applications, *Engineered Science*, 2024, **32**, 1254, doi: 10.30919/es1254.

[10] C. Papuc, G. V. Goran, C. N. Predescu, V. Nicorescu, G. Stefan, Plant polyphenols as antioxidant and antibacterial agents for shelf-life extension of meat and meat products: classification, structures, sources, and action mechanisms, *Comprehensive Reviews in Food Science and Food Safety*, 2017, **16**, 1243-1268, doi: 10.1111/1541-4337.12298.

[11] X. Sun, P. Jia, H. Zhang, M. Dong, J. Wang, L. Li, T. Bu, X. Wang, L. Wang, Q. Lu, J. Wang, Green regenerative hydrogel wound dressing functionalized by natural drug-food homologous small molecule self-assembled nanospheres, *Advanced Functional Materials*, 2022, **32**, 2106572, doi: 10.1002/adfm.202106572.

[12] S. W. Han, H. Y. Song, T. W. Moon, S. J. Choi, Influence of emulsion interfacial membrane characteristics on Ostwald ripening in a model emulsion, *Food Chemistry*, 2018, **242**, 91-97, doi: 10.1016/j.foodchem.2017.09.018.

[13] L. Qiao, L. Yuan, S. Gao, Z. Wang, Y. Tang, C. Chen, C. Zhao, X. Fu, Self-assembled nanodrug delivery systems for anti-cancer drugs from traditional Chinese medicine, *Biomaterials Science*, 2024, **12**, 1662-1692, doi: 10.1039/d3bm01451g.

[14] P. B. Dahivade, S. N. Pawar, H. M. Pathan, B. J. Lokhande, Temperature-dependent hydrothermal synthesis of CdO nanoparticles and its analysis for supercapacitor application, *ES Energy & Environment*, 2024, **24**, 1098, doi: 10.30919/esee1098.

[15] D. Xie, Y. Kuang, B. Yuan, Y. Zhang, C. Ye, Y. Guo, H. Qiu, J. Ren, S. O. Alshammari, Q. A. Alshammari, Z. M. El-Bahy, K. Zhao, Z. Guo, Q. Rao, S. Yang, Convenient and highly efficient adsorption of diosmetin from lemon peel by magnetic surface molecularly imprinted polymers, *Journal of Materials Science & Technology*, 2025, **211**, 159-170, doi: 10.1016/j.jmst.2024.06.001.

[16] G. Liu, J. Yang, Y. Wang, X. Liu, L. L. Guan, L. Chen, Protein-lipid composite nanoparticles for the oral delivery of vitamin B_12: Impact of protein succinylation on nanoparticle physicochemical and biological properties, *Food Hydrocolloids*, 2019, **92**, 189-197, doi: 10.1016/j.foodhyd.2018.12.020.

[17] M. Elhabiri, J. Hamacek, J. G. Bünzli, A.-M. Albrecht-Gary, Lanthanide homobimetallic triple-stranded helicates: insight into the self-assembly mechanism, *European Journal of Inorganic Chemistry*, 2004, **2004**, 51-62, doi: 10.1002/ejic.200300549.

[18] Y. Zou, J. Guo, S. Yin, J. Wang, X. Yang, Pickering emulsion gels prepared by hydrogen-bonded zein/tannic acid complex colloidal particles, *Journal of Agricultural and Food Chemistry*, 2015, **63**, 7405-7414, doi: 10.1021/acs.jafc.5b03113.

[19] X. Sun, P. Jia, T. Bu, H. Zhang, M. Dong, J. Wang, X. Wang, T. Zhe, Y. Liu, L. Wang, Conversional fluorescent kiwi peel phenolic extracts: Sensing of Hg^{2+} and Cu^{2+}, imaging of HeLa cells and their antioxidant activity, *Spectrochimica Acta Part A: Molecular and Biomolecular Spectroscopy*, 2021, **244**, 118857, doi: 10.1016/j.saa.2020.118857.

[20] J. Wu, X. Sun, X. Guo, M. Ji, J. Wang, C. Cheng, L. Chen, C. Wen, Q. Zhang, Physicochemical, antioxidant, *in vitro* release, and heat sealing properties of fish gelatin films incorporated with β-cyclodextrin/curcumin complexes for apple juice preservation, *Food and Bioprocess Technology*, 2018, **11**, 447-461, doi: 10.1007/s11947-017-2021-1.

[21] Y. Liu, F. Wen, H. Yang, L. Bao, Z. Zhao, Z. Zhong, The preparation and antioxidant activities of three phenyl-acylchitooligosaccharides, *Heliyon*, 2022, **8**, e10624, doi: 10.1016/j.heliyon.2022.e10624.
[22] S. U. A. Kazakhstan, S. Kabdrakhmanova, J. K. S, A. Sathian, K. Aryp, S. U. A. Kazakhstan, K. Akatan, E. Shaimardan, M. Beisebekov, T. Gulden, A. Kabdrakhmanova, S. U. A. Kazakhstan, A. Maussumbayeva, S. U. A. Kazakhstan, T. M. Joseph, S. Thomas, Anti-bacterial activity of kalzhat clay functionalized with Ag and Cu nanoparticles, *Engineered Science*, 2023, **26**, 972, doi: 10.30919/es972.
[23] S. K. Mondal, V. Perumal, R. Das, G. Roymahapatra, S. M. Mandal, Antimicrobial and anticancer activity of a novel peptide (musterolysin) extracted from slurry of mustard oil refinery industry, *ES Food & Agroforestry*, 2022, **10**, 24-29, doi: 10.30919/esfaf776.
[24] R. D. Prasad, N. R. Prasad, R. S. Prasad, N. Prasad, S. R. Prasad, M. Shrivastav, M. Gour, V. B. Kale, Z. Guo, C. B. Desai, G. M. Nazeruddin, Y. I. Shaikh, S. Banga, P. Sane, M. Saxena, J. Kamble, A review on nanotechnology from prehistoric to modern age, *ES General*, 2024, **4**, 1117, doi: 10.30919/esg1117.
[25] Q. Xu, G. Poggi, C. Resta, M. Baglioni, P. Baglioni, Grafted nanocellulose and alkaline nanoparticles for the strengthening and deacidification of cellulosic artworks, *Journal of Colloid and Interface Science*, 2020, **576**, 147-157, doi: 10.1016/j.jcis.2020.05.018.
[26] K. Li, Z. Guo, H. Li, X. Ren, C. Sun, Q. Feng, S. Kou, Q. Li, Nanoemulsion containing yellow monascus pigment: fabrication, characterization, storage stability, and lipase hydrolytic activity *in vitro* digestion, *Colloids and Surfaces B: Biointerfaces*, 2023, **224**, 113199, doi: 10.1016/j.colsurfb.2023.113199.
[27] M. S. Orellano, C. Porporatto, J. J. Silber, R. D. Falcone, N. M. Correa, AOT reverse micelles as versatile reaction media for chitosan nanoparticles synthesis, *Carbohydrate Polymers*, 2017, **171**, 85-93, doi: 10.1016/j.carbpol.2017.04.074.
[28] P. Zhang, Z. Wu, S. Zhang, L. Liu, Y. Tian, Y. Dou, Z. Lin, S. Zhang, Tannin acid induced anticorrosive film toward stable Zn-ion batteries, *Nano Energy*, 2022, **102**, 107721, doi: 10.1016/j.nanoen.2022.107721.
[29] M. L. C. Passos, M. L. M. F. S. Saraiva, Detection in UV-visible spectrophotometry: detectors, detection systems, and detection strategies, *Measurement*, 2019, **135**, 896-904, doi: 10.1016/j.measurement.2018.12.045.
[30] H. H. Kinfu, M. M. Rahman, Separation performance of membranes containing ultrathin surface coating of metal-polyphenol network, *Membranes*, 2023, **13**, 481, doi: 10.3390/membranes13050481.
[31] L. Ye, X. He, E. Obeng, D. Wang, D. Zheng, T. Shen, J. Shen, R. Hu, H. Deng, The CuO and AgO co-modified ZnO nanocomposites for promoting wound healing in Staphylococcus aureus infection, *Materials Today Bio*, 2023, **18**, 100552, doi: 10.1016/j.mtbio.2023.100552.
[32] Z. Chen, C. Wang, J. Chen, X. Li, Biocompatible, functional spheres based on oxidative coupling assembly of green tea polyphenols, *Journal of the American Chemical Society*, 2013, **135**, 4179-4182, doi: 10.1021/ja311374b.
[33] M. Chaskar, V. Kadam, C. Jagtap, N. Naik, S. Jadkar, H. Pathan, P. Adhyapak, Enhancement of photovoltaic performance of dye-sensitized solar cells using hierarchical ZnO/SnO_2 nanocomposites synthesized *via* hydrothermal method, *ES Energy & Environment*, 2024, **26**, 1250, doi: 10.30919/esee1250.
[34] A. Chaker, H. R. Alty, P. Tian, A. Kotsovinos, G. A. Timco, C. A. Muryn, S. M. Lewis, R. E. P. Winpenny, Nanoscale patterning of zinc oxide from zinc acetate using electron beam lithography for the preparation of hard lithographic masks, *ACS Applied Nano Materials*, 2021, **4**, 406-413, doi: 10.1021/acsanm.0c02756.
[35] G. Riccucci, S. Ferraris, C. Reggio, A. Bosso, G. Örlygsson, C. H. Ng, S. Spriano, Polyphenols from grape pomace: functionalization of chitosan-coated hydroxyapatite for modulated swelling and release of polyphenols, *Langmuir*, 2021, **37**, 14793-14804, doi: 10.1021/acs.langmuir.1c01930.
[36] Y. Han, J. Zhou, Y. Hu, Z. Lin, Y. Ma, J. J. Richardson, F. Caruso, Polyphenol-based nanoparticles for intracellular protein delivery *via* competing supramolecular interactions, *ACS Nano*, 2020, **14**, 12972-12981, doi: 10.1021/acsnano.0c04197.
[37] G. Li, Z. Zhuo, B. Wang, X. Cao, H. Su, W. Wang, Y. Huang, M. Hong, Constructing π-stacked supramolecular cage based hierarchical self-assemblies *via* π···π stacking and hydrogen bonding, *Journal of the American Chemical Society*, 2021, **143**, 10920-10929, doi: 10.1021/jacs.1c01161.
[38] X. Lin, H. Zhang, S. Li, L. Huang, R. Zhang, L. Zhang, A. Yu, B. Duan, Polyphenol-driving assembly for constructing chitin-polyphenol-metal hydrogel as wound dressing, *Carbohydrate Polymers*, 2022, **290**, 119444, doi: 10.1016/j.carbpol.2022.119444.
[39] J. W. Fluhr, P. M. Elias, Stratum corneum pH: formation and function of the 'acid mantle', *Exogenous Dermatology*, 2002, **1**, 163-175, doi: 10.1159/000066140.
[40] D. Xu, M. Hu, Y. Wang, Y. Cui, Antioxidant activities of quercetin and its complexes for medicinal application, *Molecules*, 2019, **24**, 1123, doi: 10.3390/molecules24061123.
[41] X. Song, Y. Wang, L. Gao, Mechanism of antioxidant properties of quercetin and quercetin-DNA complex, *Journal of Molecular Modeling*, 2020, **26**, 133, doi: 10.1007/s00894-020-04356-x.
[42] S. Liu, Y. Wang, L. Yu, J. Li, S. Ge, Development of a thermosensitive hydrogel loaded with DTT and SDF-1 facilitating *in situ* periodontal bone regeneration, *Chemical Engineering Journal*, 2022, **432**, 134308, doi: 10.1016/j.cej.2021.134308.
[43] M. M. Soliman, A. Gaber, W. F. Alsanie, W. A. Mohamed, M. M. M. Metwally, A. A. Abdelhadi, M. Elbadawy, M. Shukry, Gibberellic acid-induced hepatorenal dysfunction and oxidative stress: Mitigation by quercetin through modulation of antioxidant, anti-inflammatory, and antiapoptotic activities, *Journal of Food Biochemistry*, 2022, **46**, e14069, doi: 10.1111/jfbc.14069.
[44] K. Huang, W. Liu, W. Wei, Y. Zhao, P. Zhuang, X. Wang, Y. Wang, Y. Hu, H. Dai, Photothermal hydrogel encapsulating intelligently bacteria-capturing bio-MOF for infectious wound

healing, *ACS Nano*, 2022, **16**, 19491-19508, doi: 10.1021/acsnano.2c09593.
[45] E. H. Al-Thubaiti, Antibacterial and antioxidant activities of curcumin/Zn metal complex with its chemical characterization and spectroscopic studies, *Heliyon*, 2023, **9**, e17468, doi: 10.1016/j.heliyon.2023.e17468.
[46] S. Duan, W. Sun, P. Huang, T. Sun, X. Zhao, Y. Li, M. Yan, Tilapia gelatin films by incorporating metal-polyphenol network formed by procyanidin and zinc ion for pork preservation, *Food Packaging and Shelf Life*, 2024, **45**, 101345, doi: 10.1016/j.fpsl.2024.101345.